IOPscience iopscience.iop.org

Home Search Collections Journals About Contact us My IOPscience

Structural phase transitions in $RbFeF_4$. II. Raman scattering study

This article has been downloaded from IOPscience. Please scroll down to see the full text article.

1990 J. Phys.: Condens. Matter 2 8277

(http://iopscience.iop.org/0953-8984/2/42/006)

View the table of contents for this issue, or go to the journal homepage for more

Download details:
IP Address: 171.66.16.151
The article was downloaded on 11/05/2010 at 06:55

Please note that terms and conditions apply.

J. Phys.: Condens. Matter 2 (1990) 8277–8292. Printed in the UK

Structural phase transitions in $RbFeF_4$: II. Raman scattering study

C Pique†§, A Bulou†‖, M C Morón‡§, R Burriel§, J L Fourquet‡ and M Rousseau†

† Laboratoire de Physique de l'Etat Condensé, URA CNRS 807, Université du Maine, 72017 Le Mans Cédex, France

‡ Laboratoire des Fluorures et Oxyfluorures Ioniques, URA CNRS 449, Université du Maine, 72017 Le Mans Cédex, France

§ Instituto de Ciencia de Materiales de Aragon, CSIC-Universidad de Zaragoza, 50009 Zaragoza, Spain

Received 1 February 1990, in final form 17 July 1990

Abstract. The layer compound $RbFeF_4$, which undergoes structural phase transitions at 923 K, 416 K (second order) and 380 K (first order), has been studied by polarized Raman scattering (under the microscope) in the temperature range 473 K to 143 K. The Raman spectra were analysed with the help of a calculation of the phonon spectrum in the higher symmetry phase (phase I, $P4/mmm$) and the determination of symmetry compatibility with subgroups. The spectra collected in phase II (923–416 K) are consistent with the $P4/mbm$, $Z = 2$, symmetry resulting from the condensation of the M_3 mode. Very little changes are observed in the phase III Raman spectra, which can be explained with the $Pmmn$, $Z = 4$, space group induced by the additional condensation of X_3 modes. Below 380 K (phase IV) the Raman spectra exhibit drastic changes which are consistent with the $Pmab$, $Z = 4$, symmetry. The transition has to be imputed to the condensation of one component of the twice degenerate soft mode M_9, maintaining the condensation of one of the components of the already condensed X_3 mode, while M_3 is no longer condensed. $Pmab$ is not a $Pmmn$ subgroup, which corroborates the first-order character of the III–IV transition. The sequence of phases in $RbFeF_4$ can be schematized as $a^0a^0c^0 \rightarrow a^0a^0c^+ \rightarrow a_p^+b_p^+c^+ \rightarrow a_p^+b_p^-c^0$. It is also shown that the FeF_6 sheets can be characterized by several internal mode frequencies.

1. Introduction

$RbFeF_4$ is a layer perovskite type compound whose structures derive from the ideal $TlAlF_4$ structure (archetype) made of MF_6 octahedra centred in a tetragonal cell with monovalent A cations at the corners (figure 1). Rubidium tetrafluoroferrate has been known for a long time for its ferroelastic properties (Abrahams and Bernstein 1972, Toledano 1974). Ferroelastic domains are easily observed on platelet crystals at room temperature under polarized light. However, several space groups have been proposed for the room temperature phase. Tressaud *et al* (1969) suggested $Pca2_1$. Abrahams and Bernstein (1972) concluded it to be $Pcam$ though they obtained a better reliability with $Pca2_1$ on the basis of data from Tressaud *et al*. Finally Hidaka *et al* (1986) using four-circle x-ray diffraction measurements found $P2_12_12$ symmetry. All these solutions

‖ To whom any correspondence should be addressed.

0953-8984/90/428277 + 16 $03.50 © 1990 IOP Publishing Ltd

correspond to a unit cell $2a \times 2b \times c$ (where a, b, c represent the unit cell parameters of the ideal structure) while Deblieck *et al* (1985) observed superlattice lines by electron diffraction, which account for an additional doubling of the c dimension.

On the other hand $RbFeF_4$ exhibits three structural phase transitions at $T_{c1} = 923$ K (Tressaud *et al* 1969), $T_{c2} = 416$ K and $T_{c3} = 380$ K (Hidaka *et al* 1986). Above 923 K (phase I) $RbFeF_4$ has the ideal tetragonal structure with $P4/mmm$ symmetry and one formula unit per unit cell ($Z = 1$) (Tressaud *et al* 1969). From 923 K to 416 K (phase II), according to Hidaka *et al* (1979), the space group is $P4/mbm$ with a unit cell $\boldsymbol{a}_{II} = \boldsymbol{a} + \boldsymbol{b}$, $\boldsymbol{b}_{II} = -\boldsymbol{a} + \boldsymbol{b}$, $\boldsymbol{c}_{II} = \boldsymbol{c}$, ($Z = 2$). In phase III, from 416 K to 380 K, there is a new increase in the cell parameters ($\boldsymbol{a}_{III} = 2\boldsymbol{a}$, $\boldsymbol{b}_{III} = 2\boldsymbol{b}$, $\boldsymbol{c}_{III} = \boldsymbol{c}$); the space groups *Pmma* (Hidaka *et al* 1979) and *Pmmn* (Hidaka *et al* 1986) were proposed but no structural determination was undertaken. The room temperature phase, which appears below 380 K is denoted phase IV. As mentioned above, its structure is not clearly established. It must be noted that the most recent determination giving $P2_12_12$ symmetry (Hidaka *et al* 1986) is not consistent with the investigations of Abrahams and Bernstein (1972) who, in spite of a careful study, found no evidence for a non-centrosymmetric space group. In fact, the multidomain arrangement of the ferroelastic phase may greatly disturb the diffraction analysis.

The present Raman scattering experiments have been undertaken for the following reasons.

(i) For phases III and IV several space groups have been proposed. A Raman scattering study can help to choose between the different solutions since the Raman spectra might be inconsistent with some of them. In the present case the room-temperature ferroelastic domains are large enough to perform polarized Raman scattering studies if the experiments are performed under the microscope.

(ii) The phonon spectrum of $RbFeF_4$ can be calculated in its ideal high-temperature phase using a rigid ion model as established for $RbAlF_4$ (Bulou *et al* 1989). Then, the Raman scattering frequencies of $RbFeF_4$ can be deduced in each phase and their polarizations can be predicted using symmetry compatibility relations. Except for the modes which condense (soft modes) the frequencies are not generally very sensitive to temperature or to the crystal symmetry. In addition, the symmetry of the modes which may soften and the possible space groups for the different phases can be predicted with the calculation of the phonon spectrum.

(iii) According to Tressaud *et al* (1969) and Hidaka *et al* (1979) the following sequence of transitions is found:

$$a^0a^0c^0 \xrightarrow{923\,K} a^0a^0c^+ \xrightarrow{416\,K} a_p^+b_p^+c^+ \xrightarrow{380\,K} a_p^+b_p^+c^0.$$

Such a sequence is very uncommon since the atomic displacements responsible for the 923 K phase transition (corresponding to c^+) vanish at 380 K. The temperature behaviour of the low-frequency Raman active mode would bring important information about the mechanism of such a transition.

These investigations have been performed in connection with a diffraction study on powder and crystal at room temperature (Morón *et al* 1990, referred to as paper I in the following).

2. Experimental procedure

The $RbFeF_4$ single crystals were prepared by hydrothermal growth (Morón *et al* 1990,

paper I). They consist of about $2 \times 2 \times 0.5$ mm^3 platelets normal to the [001] axis. In some samples 0.1 mm width ferroelastic domains can be found. The orientation is facilitated by the presence of cleavage lines parallel to the [100] and [010] axes at the surface of the platelets.

The Raman scattering spectra have been collected with a Dilor Z24 Raman spectrometer equipped with a BHT Olympus microscope and a Chaix-Meca heating and cooling stage. The experiments were performed in the temperature range 473 K to 143 K with 1 K typical accuracy. The 514.5 nm line of an argon ion laser Innova 90.3 was used as the exciting source. While 900 mW laser power can be used at room temperature, above 423 K the samples are quickly damaged for laser powers over 30 mW, and above 473 K destruction occurs at too small a power to permit the collection of Raman spectra. The experiments are performed with a 50 LF objective in backscattering configuration.

3. Calculated phonon spectrum

The phonon spectrum has been predicted from an *ab initio* calculation using a rigid ion model. The interionic force constants are deduced from the isostructural compound

Table 1. Lattice and structural parameters extrapolated to 923 K from the phase II parameters and from the temperature behaviour of isostructural $RbAlF_4$. Interionic force constants A_i and ionic charges Z_i used to calculate the phonon spectrum of $RbFeF_4$ in its ideal high-temperature structure ($P4/mmm$ space group). The A_i are connected to the usual reduced units A_i' through $A_i = (e^2/8\pi\varepsilon_0 V)\, A_i'$, where V represents the volume of the unit cell. $a = b = 3.882$ Å, $c = 6.447$ Å.

	Reduced coordinates		
Atoms	x	y	z
Rb	0.5	0.5	0.5
Fe	0	0	0
F_{eq}	0.5	0	0
F_{ax}	0	0	0.279

Interaction	Distance (Å)	A_i (N m^{-1})
Fe – F_{eq}	1.941	188
Fe – F_{ax}	1.799	266
Rb – F_{eq}	3.763	1.0
Rb – F_{ax}	3.093	9.1
F_{eq} – F_{eq}	2.745	10.2
F_{eq} – F_{ax}	2.646	11.5
F_{ax} – F_{ax}	2.850	9.1

Ion	Z_i (e)
Fe	2.19
Rb	0.84
F	−0.7575

Table 2. Calculated phonon frequencies (in cm^{-1}) of $RbFeF_4$ at the Γ, M and X points of the Brillouin zone for the tetragonal ideal structure. The normal mode coordinates corresponding to these symmetries are described by Bulou *et al* (1989).

	Γ_4^i				Γ_{10}^i	
Γ_1	TO	LO	Γ_8	Γ_9	TO	LO
451	75	118	184	173	71	86
	349	363			183	188
	475	562			280	373
					496	538

M_1^i	M_3	M_4^i	M_5	M_6	M_7	M_9^i	M_{10}^i
404	95	165	409	52	329	81	80
540		468				279	195
							346

X_1^i	X_3^i	X_4^i	X_5	X_6^i	X_7^i	X_8^i
96	44	90	171	204	55	89
410	91	234		206	214	274
502	290	494		434		470

$RbAlF_4$ (Bulou *et al* 1989) and from the lattice dynamics study of FeF_3 (Daniel *et al*). They are given in table 1. The symmetry properties of the vibrations have been described by Bulou *et al* (1989). As shown below, only the modes at the Γ(000), M($\frac{1}{2}$, $\frac{1}{2}$, 0), X($\frac{1}{2}$, 0, 0) and X(0, $\frac{1}{2}$, 0) points of the Brillouin zone can become Raman active (since, according to paper I, the doubling of the *c* parameter observed by Deblieck *et al* (1985), has not been confirmed). The frequencies of these modes are given in table 2. It must be noted that the low-frequency modes are very sensitive to small variations of the force constants. They mainly concern octahedra librations and can be connected to the soft behaviour they often exhibit. As a consequence, significant differences may exist between calculated and experimental values in the low-frequency range.

4. Results

In the following, the diffusion geometry (*X*, *Y*, *Z*) for Raman polarization is labelled with respect to the crystallographic axes of the ideal high-temperature phase (***a***, ***b***, ***c***).

4.1. Raman active modes in phase I

According to Tressaud *et al* (1969), the I–II phase transition temperature is 923 K, which is far above the maximum temperature investigated in the present study. However the Raman active modes in phase I are still active in the lower temperature phases with the same polarization.

Table 3. Raman tensors expressed with respect to the crystallographic axes of the ideal high-temperature phase (***a***, ***b***, ***c***) and the corresponding symmetries expressed with respect to the crystallographic axes of phase I (D_{4h}–I), phase II (D_{4h}–II), and phases III and IV (D_{2h}).

Raman tensor	D_{4h}–I	D_{4h}–II	D_{2h}
$\begin{pmatrix} a & . & . \\ . & a & . \\ . & . & c \end{pmatrix}$	A_{1g}	A_{1g}	
			Ag
$\begin{pmatrix} a & . & . \\ . & -a & . \\ . & . & . \end{pmatrix}$	B_{1g}	B_{2g}	
$\begin{pmatrix} . & c & . \\ c & . & . \\ . & . & . \end{pmatrix}$	B_{2g}	B_{1g}	B_{1g}
$\begin{pmatrix} . & . & e \\ . & . & . \\ e & . & . \end{pmatrix}$			B_{2g}
	E_g	E_g	
$\begin{pmatrix} . & . & . \\ . & . & f \\ . & f & . \end{pmatrix}$			B_{3g}

In phase I, two modes are expected to be Raman active with $A_{1g}(\Gamma_1)$ and $E_g(\Gamma_9)$ symmetry. The Raman tensors are given in table 3 which shows that these modes can be observed in the *XX*, *YY*, *ZZ* polarizations for A_{1g} and *XZ*, *YZ* for E_g. These modes are characteristic of vibrations of octahedra disconnected along the [001] axis; they are always Raman active and intense.

The A_{1g} symmetry mode corresponds to a symmetric vibration of F_{ax} along the [001] axis (figure 4). It is always in the vicinity of 530 cm^{-1} (Bulou *et al* 1989). The ν_1 =

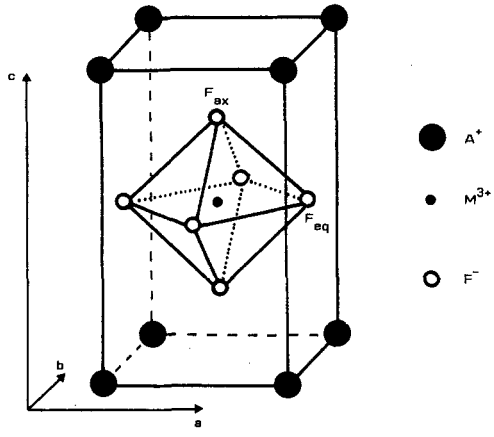

Figure 1. Tetragonal cell of the archetype structure.

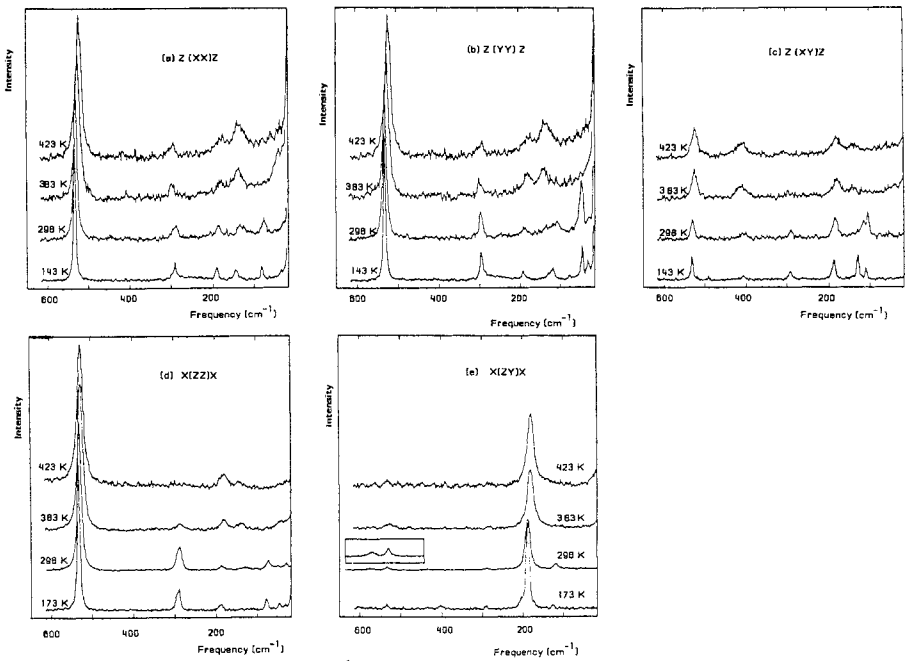

Figure 2. Some of the Raman spectra of $RbFeF_4$ collected in phase II (423 K), phase III (383 K) and phase IV (298 K and 143 K or 173 K). Figures (*a*), (*b*), (*c*) refer to experiments performed on single ferroelastic domains of phase IV in the $Z(XX)Z$, $Z(YY)Z$ and $Z(XY)Z$ geometries respectively. On the other hand the spectra represented in figures (*d*) and (*e*) are collected on multidomain samples: $X(ZZ)X$ or $Y(ZZ)Y$ (*d*); $X(ZY)X$ or $Y(ZX)Y$ (*e*).

525 cm^{-1} intense line observed at 423 K (phase II) in the $Z(XX)Z$, $X(ZZ)X$ geometries (figure 2(*a*), (*d*)) can unambiguously be attributed to this mode. Note that, according to table 2, this mode is expected to be at 451 cm^{-1}. Actually, for this mode, the F_{ax} polarizability plays a major role due to the highly asymmetric charge distribution, and the rigid ion model does not properly describe such a vibration.

The E_g mode corresponds to F_{ax} vibrations in the (001) plane and its frequency is generally in the vicinity of 200 cm^{-1} (Bulou *et al* 1983). The $\nu_2 = 178$ cm^{-1} intensity line observed at 423 K in the $X(ZY)X$ geometry (figure 2(*e*)) obviously corresponds to this mode. This is in good agreement with the calculated value (173 cm^{-1}). Note that the frequency of this mode is much higher (230 cm^{-1}) in fluoroaluminates. The lower frequency in $RbFeF_4$ probably comes from the fact that the ionic radius of the Fe ion is much larger than that of Al. Then, the distance between F_{ax} and F_{eq} is longer and their interaction and the resulting E_g frequency decrease.

4.2. Phase II

In addition to the two modes described above, the Raman spectra collected in phase II exhibit three low-intensity modes. Their characteristics at 423 K are given in table 4.

According to Hidaka *et al* (1986) the phase II space group is tetragonal, $P4/mbm$, with the new crystallographic axes $\boldsymbol{a}_{II} = \boldsymbol{a} + \boldsymbol{b}$, $\boldsymbol{b}_{II} = -\boldsymbol{a} + \boldsymbol{b}$, $\boldsymbol{c}_{II} = \boldsymbol{c}$. With such a sym-

Table 4. Raman lines characteristic of phase II.

	Frequency (423 K)	Diffusion geometry	Symmetry (a_{II}, b_{II}, c_{II})
ν_3	137	$Z(XX)Z$, $X(ZZ)X$	A_{1g}
ν_4	297	$Z(XX)Z$	B_{2g}
ν_5	407	$Z(XY)Z$	B_{1g}

metry and taking into account the 45° rotation of the crystallographic axes around *c* (table 3) the ν_3, ν_4, ν_5 lines can be attributed to A_{1g}, B_{2g} and B_{1g} symmetry modes.

In this space group seven Raman active modes can be predicted with the following symmetries:

$$2A_{1g} + B_{1g} + B_{2g} + 3E_g.$$

The Raman scattering spectra are then consistent with such a prediction.

The transition proposed above is similar to the 553 K phase transition of $RbAlF_4$ (Bulou *et al* 1989) arising from the condensation of the M_3 zone boundary mode. The new Raman active modes in phase II come from the M point modes of phase I. The compatibility relations between the symmetries in phases I and II are described in table 5.

In this space group the new A_{1g} mode (ν_3) observed at 137 cm^{-1} at 423 K comes from the M_3 condensation which corresponds to FeF_6 octahedra rotations around the tetragonal axis. Its soft behaviour (see figure 3) is consistent with such a prediction and proves the displacing character of the I–II phase transition. Of course, since it is condensed in phase II, its frequency cannot be compared to the M_3 frequency calculated in the ideal structure. the B_{1g} mode at 407 cm^{-1} and B_{2g} at 297 cm^{-1} have to be attributed to the M_5 and M_7 modes calculated at 409 cm^{-1} and 329 cm^{-1} respectively. Their normal coordinates, as deduced from Bulou *et al* (1989), are represented in figure 4. However, the two M_9 modes are not observed: M_9^1 (figure 4) is expected to have a low frequency and may even soften while the M_9^2 distortion mode should be in the vicinity of 279 cm^{-1} (table 2). The Raman lines induced by these modes may have very small intensity though the signal below 50 cm^{-1} (figure 2(*e*)) could be connected to M_9^1.

In any case the Raman scattering results are consistent with the *P*4/*mbm* space group proposed by Hidaka *et al* (1979). However, in addition to M_3 the modes M_6, M_9 and M_{10} have also a low frequency quite sensitive to the force constant values. Therefore, these three modes could condense at the M point. It has been checked that none of such condensations would give Raman spectra consistent with the experimental ones.

Table 5. Compatibility relations between the symmetries in the archetype phase and the zone centre symmetries of the phase II space group (*P*4/*mbm*) related to the Raman active modes.

$\Gamma(P4/mmm)$	$\Gamma(P4/mbm)$	$M(P4/mmm)$
$\Gamma_1 \rightarrow$	$2A_{1g}$	$\leftarrow M_3$
	B_{2g}	$\leftarrow M_7$
	B_{1g}	$\leftarrow M_5$
$\Gamma_9 \rightarrow$	3Eg	$\leftarrow 2M_9$

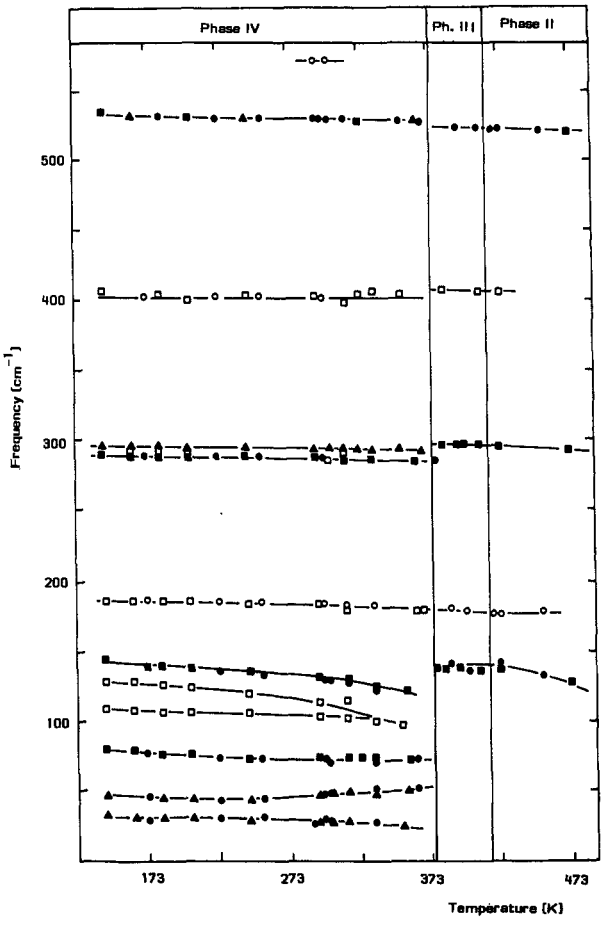

Figure 3. Temperature behaviour of the Raman active mode frequencies. The full symbols correspond to the *XX* (squares), *YY* (triangles) and *ZZ* (circles) geometries. The open squares correspond to the *XY* and the open circles to the *ZX–ZY* geometries. Full lines are only guides for the eye. The two vertical lines represent the transition temperatures.

4.3. Phase III

Only very small changes appear in the Raman spectra collected in phase III (below T_{c2} = 416 K), as can be seen in figure 2. Real changes are observed only in the near vicinity of the III–IV phase transition: a low-frequency soft band is observed in the *ZZ* and *XX* geometries and a mode appears at 286 cm^{-1} in the *ZZ* geometry. Such small changes are indeed consistent with the second-order character of the transition. However, ferroelastic domains are observed with a birefringence much smaller than the one observed in phase IV. So, the tetragonal symmetry is lost. According to Hidaka *et al* (1986), superstructure lines appear at the X points of the Brillouin zone for the ideal structure. Then, it can be thought that the II–III phase transition is a displacive transition induced by the condensation of one of the modes at the X point, in addition to the M_3 condensation that already exists in phase II. These modes, twice degenerate, are the X_1, X_3, X_4, X_7 and X_8. In the absence of a structural determination, the space groups resulting from such condensations have been determined (table 6) together with the

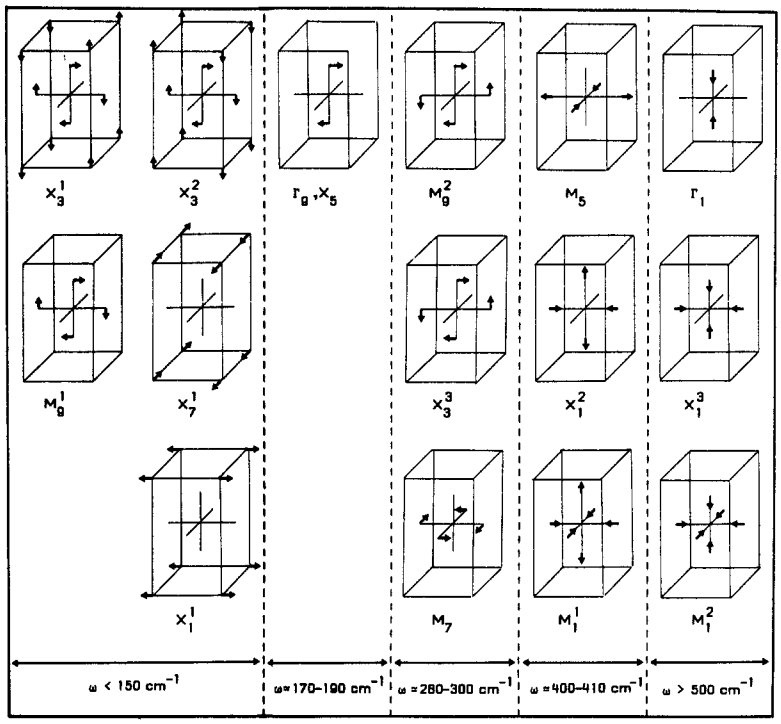

Figure 4. Normal mode coordinates of the vibrations corresponding to the Raman lines observed in $RbFeF_4$.

concomitant theoretical Raman spectra. The tetragonal groups are not consistent with the existence of ferroelastic domains. Among the remaining possibilities, only the condensation of $X_3(\begin{smallmatrix}\alpha\\ \beta\end{smallmatrix})$–*Pmmn*, $X_4(\begin{smallmatrix}\alpha\\ \beta\end{smallmatrix})$–*Pbam*, or $X_8(\begin{smallmatrix}\alpha\\ 0\end{smallmatrix})$–*Pman* are consistent with the existence of a mode with A_g symmetry in the vicinity of 286 cm^{-1}. The compatibility relations are given in table 7.

Though none of these solutions can be excluded from the Raman scattering results, it can be thought that the *Pmmn* space group proposed by Hidaka *et al* (1986) is more probable since it corresponds to FeF_6 octahedra rotations around the [100] and [010] axes such as occur in the isostructural $RbAlF_4$. Then, the II–III phase transition may reasonably be imputed to the condensation of the X_3 mode.

4.4. Phase IV

4.4.1. Experimental results. Below T_{c3} the Raman spectra exhibit drastic changes as shown in figure 2. In the *XX*, *YY* and *XY* geometries the spectra have been collected in

Table 6. Space groups resulting from the condensation of one of the X_1, X_3, X_4, X_7, X_8 twice degenerate modes of the ideal phase of $RbFeF_4$ in addition to the M_3 mode (unit cell 2***a***, 2***b***, ***c***). The other combinations would involve two transitions.

$X_3(\begin{smallmatrix}\alpha\\ \beta\end{smallmatrix})$ *Pmmn*	$X_1(\begin{smallmatrix}\alpha\\ 0\end{smallmatrix})$ *Pmam*	$X_1(\begin{smallmatrix}\alpha\\ \alpha\end{smallmatrix})$ *P4/m*
$X_4(\begin{smallmatrix}\alpha\\ \beta\end{smallmatrix})$ *Pbam*	$X_7(\begin{smallmatrix}\alpha\\ 0\end{smallmatrix})$ *Pbmm*	$X_7(\begin{smallmatrix}\alpha\\ \alpha\end{smallmatrix})$ *P4/m*
	$X_8(\begin{smallmatrix}\alpha\\ 0\end{smallmatrix})$ *Pman*	$X_8(\begin{smallmatrix}\alpha\\ \alpha\end{smallmatrix})$ *P4/n*

Table 7. Compatibility relations between the symmetries in the archetype phase and the zone centre symmetries of the possible space groups of phase III.

Pmmn ($X_3(\begin{smallmatrix}\alpha\\ \beta\end{smallmatrix})$)	*Pbam* ($X_4(\begin{smallmatrix}\alpha\\ \beta\end{smallmatrix})$)	*Pman* ($X_8(\begin{smallmatrix}\alpha\\ 0\end{smallmatrix})$)
$\Gamma_1 \rightarrow 9Ag \leftarrow \begin{matrix}\swarrow M_7\\ M_3\\ \nwarrow 3X_3(2)\end{matrix}$	$\Gamma_1 \rightarrow 9Ag \leftarrow \begin{matrix}\swarrow M_7\\ M_3\\ \nwarrow 3X_4(2)\end{matrix}$	$\Gamma_1 \rightarrow 6Ag \leftarrow \begin{matrix}\swarrow M_7\\ M_3\\ \nwarrow 3X_8(2)\end{matrix}$
$5B_{1g} \leftarrow \begin{matrix}\swarrow M_5\\ 2M_1\\ \nwarrow X_5(2)\end{matrix}$	$9B_{1g} \leftarrow \begin{matrix}\swarrow M_5\\ 2M_1\\ \nwarrow 3X_6(2)\end{matrix}$	$6B_{1g} \leftarrow \begin{matrix}\swarrow\\ 2M_1\\ \nwarrow M_5(2)\end{matrix}$
$\Gamma_9 \begin{matrix}\nearrow 8B_{2g} \leftarrow 3X_{1(2)}\\ \searrow 8B_{3g} \leftarrow 2X_{7(2)}\end{matrix}$ $2M_{9(2)}$	$\Gamma_9 \begin{matrix}\nearrow 6B_{2g} \leftarrow 2M_9(2)\\ \searrow 6B_{3g} \leftarrow 3X_8(2)\end{matrix}$	$\Gamma_9 \begin{matrix}\nearrow 9B_{2g} \leftarrow 3X_4(2)\\ \searrow 9B_{3g} \leftarrow 3X_6(2)\end{matrix}$ $2M_9(2)$

single domains selected under polarized light. The *X* and *Y* labelling is arbitrary since, due to the multidomain arrangement and the small domain size, the ***a*** and ***b*** crystallographic axes cannot be identified by x-ray diffraction. However, they can be easily characterized by polarized Raman scattering since the *XX* and *YY* Raman spectra look very different (figures 2(*a*)–(*b*)). The results obtained at room temperature and at the lowest temperature investigated (143 K in the *XX*, *YY* and *XY* geometries and 173 K in the *ZZ* and *ZX–ZY* geometries) are reported in table 8.

The higher frequency mode (L1) is observed only in the *ZX–ZY* configuration at about 573 cm^{-1} at room temperature. The L2 line observed in the *XX*, *YY* and *ZZ* configurations at 531 cm^{-1} at room temperature unambiguously corresponds to the Γ_1 line characteristic of the structure. The signal observed at the same frequency in the *XY* and *ZX–ZY* configurations obviously comes from contamination. The L3 line is observed in the *XY* and *ZX–ZY* configurations. Due to their weakness none of the two signals can be imputed to contamination and consequently two lines with different symmetries exist. Several lines appear in the frequency range 280–300 cm^{-1}. The L4 line in *YY* is

Table 8. Raman line frequencies of $RbFeF_4$ in the different geometries at room temperature and at the lowest temperature investigated (143 K in the *XX*, *YY* and *XY* geometries, 173 K in the *ZZ* and *ZX–ZY* geometries). The symbol 's' stands for small signal.

	XX		*YY*		*ZZ*		*XY*		*ZX–ZY*	
T (K)	143	298	143	298	173	298	143	298	173	298
L1	—	—	—	—	—	—	—	—	—	573
L2	535	531	534	531	532	530	533	531	532	530
L3	—	—	—	—	—	—	407	403	404	402
L4	s	s	297	295	s	s	—	—	—	—
L5	291	~287	s	s	290	288	291	289	290	287
L6	191	~185	193	~187	~188	~188	187	183	188	184
L7	145	~133	—	—	—	—	—	—	—	—
L8	—	s	—	s	—	130	—	—	—	—
L9	—	—	—	—	—	—	129	113	126	116
L10	—	—	~117	~107	—	—	—	—	—	—
L11	—	—	—	—	—	—	109	105	—	—
L12	81	75	—	—	78	74	—	—	—	—
L13	—	—	47	47	~46	48	—	—	—	—
L14	~33	~25	~33	~29	30	30	—	—	—	—

observed at a somewhat higher frequency than the L5 line in *XX* geometry, so we estimate that two lines are present. Actually the slight asymmetry of these two lines is consistent with this conclusion. In the *ZZ* geometry the line observed in this region is mainly L5. In the *XY* geometry a line is also observed at 291 cm^{-1}. It has a similar intensity to the L2 line (contamination) while in the *XX* geometry the L5 line is much smaller than the L2 line. Then, one can infer that the L5 line observed in the *XY* geometry really exists and is different from the L5 line observed in the *XX* and *ZZ* geometries. On the other hand the L5 line observed in the *ZX–ZY* geometry is very small and may be attributed to contamination.

The L6 lines in the *XX*, *YY* and *ZZ* configurations may be due to contamination by the intense Γ_9 line characteristic of the structure observed in the *ZX–ZY* configuration though this conclusion is not certain. However, the L6 line observed in the *XY* configuration could be real since in this configuration it is more intense than in the *XX* and *YY* geometries, while the orientation with respect to *Z* is unchanged.

In the frequency range 150–100 cm^{-1} the situation is still more confused. The L7 line observed in the *XX* geometry really softens but becomes asymmetrical at room temperature. The L8 line (*ZZ*) observed at room temperature disappears at low temperatures. The L9 line observed in the *XY* geometry undergoes a real softening and its intensity greatly increases at low temperature (it is also observed in the *ZX–ZY* geometry). On the other hand the frequency of the L11 line observed in the same geometry is not temperature dependent but its intensity decreases on cooling. The line L10 appears as a broad asymmetrical band with a slightly soft character. The L12 line is observed in the *XX* and *ZZ* geometries and its intensity decreases when the transition is approached. On the other hand the L13 line observed in the *YY* geometry appears as a very intense line not temperature dependent. On cooling from the transition to room temperature the frequency decreases (from 51 cm^{-1} to 46 cm^{-1}) and then remains constant down to the lowest temperatures. Finally a last line (L14) is observed in *YY* and *ZZ* geometries in the vicinity of 30 cm^{-1} with a soft character.

To summarize, the following experimental results are found with respect to the D_{2h} symmetry, which is the highest symmetry expected for this phase

A_g : L2(Γ_1), L4, L5, L7, L12, L13, L14

B_{1g} : L3, L5, L6, L9, L11

B_{2g}, B_{3g} : L1, L3, L6(Γ_9).

The L8 line which disappears at low temperatures may be imputed to a two phonon process such as occurs in $RbAlF_4$ (Bulou *et al* 1989). The temperature behaviour of these lines' frequencies is plotted in figure 3.

The following remarks have to be made with respect to the spectra collected in phases II and III:

(i) The M_3 line in phases II and III vanishes in phase IV near the transition. The L7 line in the same frequency range has another origin than the M_3 mode.

(ii) The line at 407 cm^{-1} in phases II and III attributed to M_5 largely decreases in intensity in phase IV and seems to be shifted to a lower frequency. Then, it may have a different origin in phase IV.

4.4.2. Assignations in the Pmab space group. According to paper I there is only one orthorhombic centrosymmetric space group consistent with the extinction rules found from oscillation or Weissenberg photographs, the *Pmab* space group.

Table 9. The four different *Pmab* subgroups of the *P4/mmm* archetype (with the origin taken at the Fe position) and the compatibility relations for the Raman active modes. The numbers of components involved when the modes are twice degenerate are given in parentheses.

	A	B	C	D
Generators	$\{\sigma_x\|000\}\{\sigma_y\|\frac{1}{2}\frac{1}{2}0\}\{\sigma_z\|0\frac{1}{2}0\}$	$\{\sigma_x\|000\}\{\sigma_y\|\frac{1}{2}\frac{1}{2}0\}\{\sigma_z\|0\frac{1}{2}0\}$	$\{\sigma_x\|\frac{1}{2}00\}\{\sigma_y\|\frac{1}{2}00\}\{\sigma_z\|0\frac{1}{2}0\}$	$\{\sigma_x\|\frac{1}{2}00\}\{\sigma_y\|\frac{1}{2}\frac{1}{2}0\}\{\sigma_z\|0\frac{1}{2}0\}$
A_g	$\Gamma_1 + 2M_9(1) + 3X_4(1) + 3X_8(1)$	$\Gamma_1 + 2M_4 + 3X_3(2) + 3X_4(2)$	$\Gamma_1 + M_6 + 2X_7(2) + 3X_8(2)$	$\Gamma_1 + 2M_9(1) + 3X_3(1) + 2X_7(1)$
B_{1g}	$2M_9(1) + 3X_6(1)$	$M_6 + X_5(2) + 3X_6(2)$	$2M_4 + 3X_1(2)$	$2M_9(1) + 3X_1(1) + X_5(1)$
B_{2g}	$\Gamma_9(1) + M_3 + M_7 + 3X_4(1)$	$\Gamma_9(1) + 3M_{10}(1) + 2X_7(2)$	$\Gamma_9(1) + 3M_{10}(1) + 3X_4(2) + X_5(2)$	$\Gamma_9(1) + 2M_1 + M_5 + X_5(1) + 2X_7(1)$
B_{3g}	$\Gamma_9(1) + 2M_1 + M_5 + 3X_6(1) + 3X_8(1)$	$\Gamma_9(1) + 3M_{10}(1) + 3X_1(2) + 3X_8(2)$	$\Gamma_9(1) + 3M_{10}(1) + 3X_3(2) + 3X_6(2)$	$\Gamma_9(1) + M_3 + M_7 + 3X_1(1) + 3X_3(1)$

Though the III–IV phase transition is a first order one, the hysteresis (if any) is small and the crystals are not damaged so that the *Pmab* has to be searched among subgroups of *P4/mmm* describing the archetype symmetry. In the phase IV unit cell, $2a \times 2b \times c$ (where a, b, c represent the cell parameters of the archetype), four different solutions are found (table 9) depending on the position of the mirror planes with respect to the Fe ions, taken at the origin as in the archetype phase. It can be verified with the help of the calculated spectrum (table 2) that none of the A, B and C solutions are able to explain the experimental results since, for example, in the low-frequency range (below 150 cm^{-1}) only three A_g and one B_{1g} symmetry modes should be expected while four and two respectively are observed. On the other hand an assignation is possible on the basis of the D solution which corresponds to the case where the Fe ions are at a symmetry centre. The proposed assignation is the following:

A_g symmetry lines. The lines with A_g symmetry arise from Γ_1, M_9, X_3 and X_7 symmetry modes. The L2 line is obviously assigned to the Γ_1 mode. The L4 and L5 can unambiguously be assigned to X_3 and M_9 octahedra distortion modes calculated at 290 and 279 cm^{-1} respectively. This is consistent with the presence of a B_{1g} mode (L5) in the same frequency range since the M_9 modes split into A_g and B_{1g} modes. The low-frequency mode L13, which does not show a real soft character, should be assigned to the Rb translatory mode X_7; the large intensity of this mode may be related to the fact that it is connected to vibrations of a polarizable ion which undergoes large static displacements. The assignation of the three other lines is not so easy, although, by comparison to $RbAlF_4$, the L12 line may arise from the second X_3 mode calculated at 91 cm^{-1}. Then, the L14 and L7 lines would be assigned to the low-frequency soft modes X_3 and M_9 respectively.

B_{1g} symmetry lines. The lines with B_{1g} symmetry arise from M_9, X_1 and X_5 symmetry modes. The L5 line has already been attributed to the M_9 mode and the L3 line frequency is only consistent with the X_1 mode calculated at 410 cm^{-1}. This assignation is also consistent with the existence of a mode in B_{2g}–B_{3g} symmetry at the same frequency since X_1 splits into B_{1g} and B_{3g} modes. The soft L9 line is then attributed to the low-frequency M_9 mode which is expected to have a soft character. Note that, as often observed, its frequency is smaller than the frequency of the corresponding mode with A_g symmetry ('condensed' component). The L11 line is attributed to the X_1 mode calculated at 96 cm^{-1} and the L6 line (if it is not a contamination) could be explained by the X_5 mode.

B_{2g}–B_{3g} symmetries. The L6 line is unambiguously assigned to the Γ_9 mode. The L1 line would be due either to M_1 (calculated at 540 cm^{-1}) or to X_1 (calculated at 502 cm^{-1}). The L3 line can arise from X_1 (calculated at 410 cm^{-1}) which is also active in B_{1g} symmetry or from M_1 (calculated at 404 cm^{-1}) or even M_5 (calculated at 409 cm^{-1}). Note that the line observed in the same frequency range in phases II and III was attributed to this mode and that it shifts to a lower frequency and decreases in intensity at the III–IV transition.

These results show that the Raman spectra can be explained by the *Pmab* symmetry.

4.4.3. Assignations in the $P2_1ab$ and the $P2_12_12_1$ space group. The $P2_1ab$ space group, a subgroup of *Pmab*-D solution, has also been considered. Since it is a subgroup of the *Pmab*-D solution the assignation proposed above is still consistent with the $P2_1ab$ space group. However, a larger number of Raman active modes are expected.

The compatibility relations have also been established under the hypothesis (not confirmed in paper I) of the $P2_12_12$ space group for phase IV and taking the origin

according to Hidaka *et al* (1986). It appears that all the modes (except the acoustic ones) are Raman active. Then, the Raman study cannot prove if this space group is the wrong one even though the number of lines is much smaller than expected. However, it must be noted that none of the M_6 or X_7 modes, which may be responsible for the L13 line, would appear in the A symmetry.

4.4.4. Discussion. To conclude, the *Pmab* space group for phase IV explains both the diffraction results and the main lines of the Raman spectra. For the existence of this space group the compatibility relations require the condensation of two of the three possible modes $M_9(\begin{smallmatrix}\alpha\\-\alpha\end{smallmatrix})$, $X_3(\begin{smallmatrix}\alpha\\0\end{smallmatrix})$ and $X_7(\begin{smallmatrix}0\\\beta\end{smallmatrix})$. The assignations proposed show that the lines which exhibit a soft character arise from the lower frequency M_9 and X_3 modes. So, since in phase III the X_3 lower frequency mode is already condensed, the III–IV phase transition could be connected to a condensation of the M_9 mode (one of the two components). This is an octahedra tilt mode around the [010] axis. Such a condensation has already been observed in the mixed compounds $K_{1-x}Rb_xAlF_4$ (Launay *et al* 1987) in addition to M_3 and X_3 condensations giving rise to the $P2_1/m$ space group. The uncommon behaviour encountered in $RbFeF_4$ is the disappearance in phase IV of the M_3 condensation existing in phases II and III (this is evidenced by the fact that M_3 loses the A_g symmetry) and additionally the disappearance of one of the two X_3 components condensed in phase III. Such a result has been checked by the attempt to refine the structure in the $P2_1/m$ space group, isotranslational subgroup of *Pmab*, in which M_3 is condensed (paper I). The poor reliability obtained for this refinement gives confidence to the interpretation of the disappearance of the M_3 condensation. Note that according to the behaviour of the $\frac{5}{2}\,\frac{3}{2}\,1$ diffraction line (Hidaka *et al* 1986) the decreasing of the tilt angle around the [001] axis (corresponding to M_3) begins in phase III. The sudden vanishing of the M_3 Raman line intensity at the III–IV phase transition is consistent with the symmetry change for this line. However, in phase IV, this mode is expected in the B_{3g} symmetry. Though the L9 line in the *ZY* geometry, which exhibits a soft character, could be attributed to this line, a contamination by the B_{1g} mode seems to be more probable. In any case these results establish that the tilt angle around [001] disappears in phase IV. Then, phase IV can be described by the tilt system $a_p^+ b_p^- c^0$.

The ionic displacements corresponding to the assignations proposed in the different phases are shown in figure 4. It appears that the four high-frequency bands (180 cm^{-1}; 290 cm^{-1}, 400 cm^{-1}, 530 cm^{-1}) which are evidenced in figure 3 can be attributed to four kinds of vibrations of octahedra that do not depend strongly on the $\boldsymbol{k}$ wave vector. Then, the structural phase transitions of $RbFeF_4$ reveal the characteristic frequencies of the vibrations of FeF_6 octahedra connected in a two-dimensional array.

5. Conclusion

The polarized Raman scattering spectra of ferroelastic $RbFeF_4$ have been collected in the three phases II, III and IV. On the basis of the calculation of the phonon spectrum in the archetype phase (phase I) together with the establishment of compatibility relations, it has been possible to determine which space groups are consistent with the Raman spectra and to point out which instabilities could be responsible for the three transitions.

The Raman spectra collected in phase II are only consistent with the $P4/mbm$ space group as proposed by Hidaka *et al* (1986). The I–II transition can be imputed to the

condensation of the M_3 zone boundary mode which exhibits a softening. This is an octahedra vibration around the [001] axis and phase II can be described by the tilt system $a^0a^0c^+$.

In phase III only one additional A_g symmetry line is unambiguously observed. According to the phonon spectrum three space groups could be expected: *Pmmn*, *Pbam* and *Pman*. However, the *Pmmn* space group, as proposed by Hidaka *et al* (1986) seems to be more probable since it is induced by the condensation of an octahedra tilt mode around the [100] and [010] axes (X_3 mode). The corresponding tilt system should be $a_p^+b_p^+c^+$. Such a sequence of transition ($a^0a^0c^0 \rightarrow a^0a^0c^+ \rightarrow a_p^+b_p^+c^+$) has already been found in $RbAlF_4$.

Drastic changes appear in the Raman spectra of phase IV where many new lines are observed. According to paper I the corresponding space group is *Pmab* and the Raman spectra are consistent with this symmetry. In this framework the III–IV phase transition can be related to the condensation of the M_9 octahedra tilt mode around the [010] axis together with the disappearance of the M_3 condensation and one of the components of the condensed X_3 mode. This phase can also be described by a tilt system scheme $a_p^+b_p^-c^0$. The phase IV space group is not a subgroup of the phase III one, therefore, such a transition can only be first order as is experimentally found. The disappearance of the condensation responsible for the I–II structural phase transition is an uncommon feature. Such behaviour preserves a high symmetry in spite of multiple condensations.

The use of both diffraction and Raman scattering has made it possible to shed some light on the $RbFeF_4$ phase IV symmetry for which several space groups were proposed. Moreover, it appears that the model used to calculate the phonon spectrum, which involves a small number of parameters deduced from other structures, gives fairly good results. The frequencies and eigenvectors characteristic of the FeF_6 vibrations in such layered structures have been deduced. These data are useful to investigate the dynamic properties of more complicated structures like, for example, the potassium tetrafluoroferrate in which an incommensurate phase has been predicted.

Acknowledgments

The authors would like to thank P Daniel for preliminary results on the interaction constants in the iron–fluorine system. This work was supported by a grant from the Spanish–French Committee for Scientific Cooperation. One of the authors (M C Morón) is grateful for the receipt of a Nato Postdoctoral fellowship and financial support given by CNRS, France.

References

Abrahams S C and Bernstein J L 1972 *Mater. Res. Bull.* **7** 715–20
Bulou A, Rousseau M, Nouet J and Hennion B 1989 *J. Phys.: Condens. Matter* **1** 4553–83
Bulou A, Rousseau M, Nouet J, Loyzance P L, Mokhlisse R and Couzi M 1983 *J. Phys. C: Solid State Phys.* **16** 4527–37
Daniel P, Bulou A, Rousseau M and Nouet J *Phys. Rev.* B at press
(submitted)
Deblieck R, Van Landuyt J and Amelinckx S 1985 *J. Solid State Chem.* **59** 379–87
Hidaka M, Akiyama H and Wanklyn B M 1986 *Phys. Status Solidi* **97** 387–95
Hidaka M, Wood I G, Wanklyn B M and Garrard B J 1979 *J. Phys. C: Solid State Phys.* **12** 1799–807

Launay C, Bulou A and Nouet J 1987 *Solid State Commun.* **69** 539–41
Morón M C, Bulou A, Piqué C and Fourquet J L 1990 *J. Phys.: Condens. Matter* **2** 8269–75
Toledano J C 1974 *Ann. Telecomm.* **29** 249–70
Tressaud A, Galy J and Portier J 1969 *Bull. Soc. Franc. Min.* **92** 335–41